Eur. Phys. J. C 16, 349–359 (2000)
Digital Object Identifier (DOI) 10.1007/s100520000199

THE EUROPEAN PHYSICAL JOURNAL C

Implications of color-string percolation on multiplicities, correlations, and the transverse momentum

M.A. Braun[1], C. Pajares[2]

[1] High-Energy Physics Department, S. Petersburg University, 198904 St. Petersburg, Russia
[2] Departamento de Física de Partículas, Universidade de Santiago de Compostela, 15706-Santiago de Compostela, Spain

Received: 13 July 1999 / Published online: 8 June 2000 – © Springer-Verlag 2000

Abstract. In the color-string model, the impact of string percolation on multiplicities, $\langle p_{\mathrm{T}}^2 \rangle$, and their long-range (forward–backward) correlations is studied. It is assumed that different string overlaps produce the observed hadrons independently. The multiplicities are shown to be damped by a simple factor which follows from the percolation theory. The $\langle p_{\mathrm{T}}^2 \rangle$ rise at the same rate as multiplicities fall. A clear signature of the percolation phase transition is found to be the behavior of the forward–backward correlations for intensive quantities, such as $\langle p_{\mathrm{T}}^2 \rangle$ or its inverse, which can be detected in the relativistic heavy-ion collider.

1 Introduction

Multiparticle production at high energies is currently (and successfully) described in terms of color strings stretched between the projectile and target [1–6]. Hadronization of these strings produces the observed hadrons. Color strings may be viewed as (small) areas in the transverse space filled with color field created by the colliding partons. Particles are created via emission of $\mathrm{q\bar{q}}$ pairs in this field. With growing energy and/or atomic number of colliding particles, the number of strings grows. Once strings have a certain nonzero dimension in the transverse space they start to overlap, forming clusters, very much like disks in the two-dimensional percolation theory. The geometrical behavior of strings in the transverse plane then follows that of percolating discs. In particular, at a certain critical string density a macroscopic cluster appears (that is infinite in the thermodynamic limit), which marks the percolation phase transition [7–9].

The percolation theory governs the geometrical pattern of the string clustering. Its observable implications, however, require introduction of some dynamics to describe string interaction, i.e., the behavior of a cluster formed by several overlapping strings.

One can study several different possibilities.

The most naive attitude is to assume that nothing happens as strings overlap; in other words, they continue to emit particles independently without being affected by their overlapping neighbors. This is a scenario of noninteracting strings that closely corresponds to original calculations in the color-string approach, oriented at comparatively small energies (and numbers of strings). However, this scenario contradicts the idea that strings are areas of the transversal space filled with color field and thus with energy, since in the overlapping areas the energy should have grown.

In another limiting case, one may assume that a cluster of several overlapping strings behaves as a single string with an appropriately higher color field (a string of higher color, or a "color rope". [10]). This fusion scenario was proposed by the authors and later realized as a Monte Carlo algorithm nearly a decade ago [11,12]. It predicts lowering of total multiplicities and forward–backward correlations (FBC) and also strange-baryon enhancement, all of which are in reasonable agreement with the known experimental trends.

However, both discussed scenarios are obviously of a limiting sort. In a typical situation, strings overlap only partially, and there is no reason to expect them to fuse into a single stringy object, especially if the overlap is small. The transverse space occupied by a cluster of overlapping strings splits into a number of areas in which different numbers of strings overlap, including areas where no overlapping takes place. In each such area color fields coming from the overlapping strings will add together. As a result, the total cluster area is split in domains with different color- field strength. As a first approximation, neglecting the interaction at the domain frontiers, one may assume that emission of $\mathrm{q\bar{q}}$ pairs in the domains proceeds independently, governed by the field strength ("the string tension") in a given domain. This picture implies that clustering of strings actually leads to their proliferation, rather than fusion, since each particular overlap may be considered as a separate string. Evidently newly formed strings differ not only in their colors but also in their transverse areas.

As a simple example, consider a cluster of two partially overlapping strings (Fig. 1). One distinguishes three different regions: regions 1 and 2, where no overlapping takes place and the color field remains the same as in a single string, and the overlap region 3 with color fields of

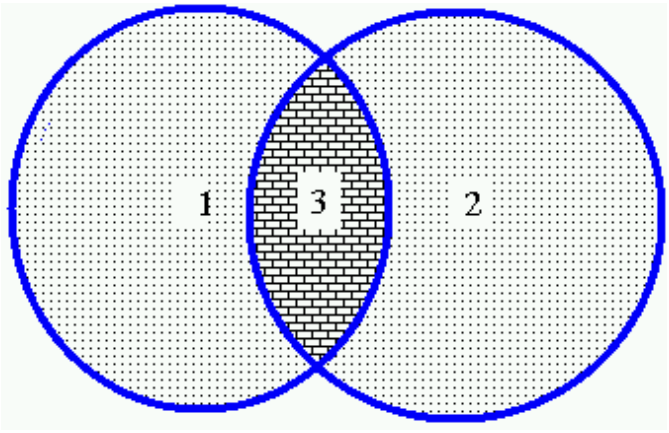

Fig. 1. Projections of two overlapping strings onto the transverse plane

both strings summed. In our picture, particle production will proceed independently from these three areas, that is from three different strings corresponding to areas 1, 2, and 3. In this sense, string interaction has split two strings into three of different color, area, and form in the transverse space.

We stress that these dynamical assumptions are rather independent of the geometrical picture of clusterization. In particular, in each of the scenarios discussed above, at a certain string density there occurs the percolation phase transition. However its experimental signatures crucially depend on the dynamical contents of string interaction. With no interaction, clustering does not change physical observables, so that the geometric percolation will not be felt at all. With the interaction between strings turned on, clustering (and percolation) lead to well observable implications.

In this paper, we shall study these implications for the simplest observables, such as multiplicities, average transverse momenta, and FBC, in the realistic scenario discussed above, which corresponds to independent particle production from different overlap domains. Our choice of observables is dictated by the possibility of relating them directly to the domain properties without introducing any more assumptions.

2 Multiplicity and $\langle p_{\rm T}^2\rangle$ for overlapping strings

As was stated in the introduction, the central dynamical problem is to find how the observables change when several strings form a partially overlapping cluster. In the overlap areas the color fields of individual strings are summed together. It is more convenient to sum the charges which generate the color field of overlapping strings.

Let only two strings, each of area σ_0 in the transverse space, partially overlap in the area S_2 (region 3 in Fig. 1), so that $S_1 = \sigma_0 - S_2$ is the area in each string not overlapping with the other. In the following, it will be called the overlap area of one string. A natural assumption seems to be that the average color density ξ of the string in the transverse plane is a constant,

$$\xi = Q_0/\sigma_0, \tag{1}$$

where Q_0 is a color of the string. For partially overlapping strings, the color in each of the two nonoverlapping areas will then be

$$Q_1 = \xi S_1 = Q_0(S_1/\sigma_0). \tag{2}$$

The color in the overlap area Q_2 will be a vector sum of the two overlapping colors ξS_2. In this summation, the total color squared should be conserved [10]. Indeed, $Q_2^2 = (\mathbf{Q}_{\rm ov}+\mathbf{Q}'_{\rm ov})^2$ where $\mathbf{Q}_{\rm ov}$ and $\mathbf{Q}'_{\rm ov}$ are the two vector colors in the overlap area. Since the colors in the two strings may generally be oriented in an arbitrary manner respective to one another, the average of $\mathbf{Q}_{\rm ov}\mathbf{Q}'_{\rm ov}$ is zero. Then $Q_2^2 = Q_{\rm ov}^2 + {Q'_{\rm ov}}^2$, which leads to

$$Q_2 = \sqrt{2}\,\xi S_2 = \sqrt{2}\,Q_0(S_2/\sigma_0). \tag{3}$$

One observes that because of its vector nature, the color in the overlap is less than the sum of the two overlapping colors. This phenomenon was first mentioned in [10] for the so-called color ropes.

The two simplest observables, the multiplicity μ and the average transverse momentum squared $\langle p_{\rm T}^2\rangle$, are directly related to the field strength in the string and thus to its generating color. In fact they are both proportional to the color [10,13]. Thus, assuming independent emission from the three regions 1, 2, and 3 in Fig. 1, we get for the multiplicity:

$$\mu/\mu_0 = 2(S_1/\sigma_0) + \sqrt{2}\,(S_2/\sigma_0), \tag{4}$$

where μ_0 is a multiplicity for a single string. To find $\langle p_{\rm T}^2\rangle$, one has to divide the total transverse momentum squared of all observed particles by the total multiplicity. In this way, for our cluster of two strings, we obtain

$$\begin{aligned}\langle p_{\rm T}^2\rangle/\langle p_{\rm T}^2\rangle_0 &= \frac{2(S_1/\sigma_0) + \sqrt{2}\sqrt{2}\,(S_2/\sigma_0)}{2(S_1/\sigma_0) + \sqrt{2}\,(S_2/\sigma_0)}\\ &= \frac{2}{2(S_1/\sigma_0) + \sqrt{2}\,(S_2/\sigma_0)},\end{aligned} \tag{5}$$

where $\langle p_{\rm T}^2\rangle_0$ is the average transverse momentum squared for a single string and we have used the evident property $2S_1 + 2S_2 = 2\sigma_0$ in the second equality.

Generalizing to any number N of overlapping strings, we find the total multiplicity as

$$\mu/\mu_0 = \sum_i \sqrt{n_i}\,(S^{(i)}/\sigma_0), \tag{6}$$

where the sum goes over all individual overlaps i of n_i strings having areas $S^{(i)}$. Similarly for the $\langle p_{\rm T}^2\rangle$, we obtain

$$\begin{aligned}\langle p_{\rm T}^2\rangle/\langle p_{\rm T}^2\rangle_0 &= \frac{\sum_i n_i\,(S^{(i)}/\sigma_0)}{\sum_i \sqrt{n_i}\,(S^{(i)}/\sigma_0)}\\ &= \frac{N}{\sum_i \sqrt{n_i}\,(S^{(i)}/\sigma_0)}.\end{aligned} \tag{7}$$

In the second equality, we again use an evident identity $\sum_i n_i S^{(i)} = N\sigma_0$. Note that (6) and (7) imply a simple relation between the multiplicity and transverse momentum

$$\frac{\mu}{\mu_0}\frac{\langle p_{\rm T}^2\rangle}{\langle p_{\rm T}^2\rangle_0} = N, \tag{8}$$

which evidently means conservation of the total transverse momentum produced.

Equations (6) and (7) do not appear to be easy to apply. To calculate the sums over i, one seems to have to identify all individual overlaps of any number of strings with their areas. For a large number of strings, the latter may have very complicated forms, and their analysis presents great calculational difficulties. However, one immediately recognizes that such individual tracking of overlaps is not at all necessary. One can combine all terms with a given number of overlapping strings $n_i = n$ into a single term, which sums all such overlaps into a total area of exactly n overlapping strings S_n. Then one finds, instead of (6) and (7),

$$\mu/\mu_0 = \sum_{n=1}^{N} \sqrt{n}\,(S_n/\sigma_0) \tag{9}$$

and

$$\langle p_{\rm T}^2\rangle/\langle p_{\rm T}^2\rangle_0 = \frac{N}{\sum_{n=1}^{N}\sqrt{n}\,(S_n/\sigma_0)}. \tag{10}$$

In contrast to individual overlap areas $S^{(i)}$, the total ones S_n can be easily calculated (see the appendix). Let the projections of the strings onto the transverse space be distributed uniformly in the interaction area S with a density ρ. We introduce a dimensionless parameter

$$\eta = \rho\sigma_0 = N\sigma_0/S. \tag{11}$$

The "thermodynamic limit" corresponds to taking the number of the strings $N \to \infty$ and keeping η fixed. In this limit, one readily finds that the distribution of the overlaps of n strings is Poissonian, with a mean value η:

$$p_n = \frac{S_n}{S} = \frac{\eta^n}{n!}{\rm e}^{-\eta}. \tag{12}$$

From (9) we then find that the multiplicity is damped because of overlapping by a factor

$$F(\eta) = \frac{\mu}{N\mu_0} = \frac{\langle\sqrt{n}\rangle}{\eta}, \tag{13}$$

where the average is taken over the Poissonian distribution (12).

The behavior of $F(\eta)$ is shown in Fig. 2. It smoothly goes down from unity at $\eta = 0$ to values around 0.5 at $\eta = 4$, falling as $1/\sqrt{\eta}$ for larger η. According to (10), the inverse of F shows the rise of $\langle p_{\rm T}^2\rangle$. Note that a crude estimate of $F(\eta)$ can be done from the overall compression of the string area due to overlapping. The fraction of the total area occupied by the strings according to (12) (see also [14]) is given by

$$\sum_{n=1} p_n = 1 - {\rm e}^{-\eta}. \tag{14}$$

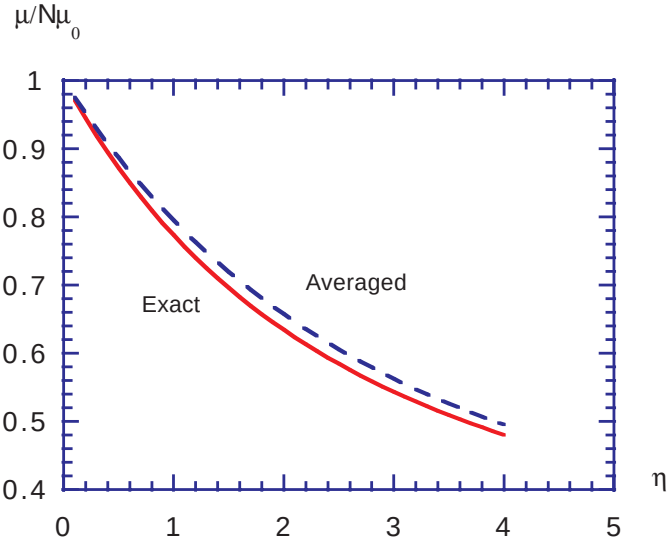

Fig. 2. Damping of the multiplicity as a function of η

The compression is given by (14) divided by η. According to our picture, the multiplicity is damped by the square root of the compression factor, so that the damping factor is

$$F(\eta) = \sqrt{\frac{1-{\rm e}^{-\eta}}{\eta}}. \tag{15}$$

For all the seeming crudeness of this estimate, (15) is very close to the exact result as shown in Fig. 2 by a dashed curve.

3 Percolation

Percolation is a purely classical mechanism. Overlapping strings form clusters. At some critical value of the parameter η, a phase transition of the 2nd order occurs: A cluster appears which extends over the whole surface (an infinite cluster in the thermodynamic limit). The critical value of η is found to be $\eta_{\rm c} \simeq 1.12$–1.20 [15]. Below the phase transition point, for $\eta < \eta_{\rm c}$, there is no infinite cluster. Above the transition point, at $\eta > \eta_{\rm c}$ an infinite cluster appears with a probability

$$P_\infty = \theta(\eta-\eta_{\rm c})(\eta-\eta_{\rm c})^\beta. \tag{16}$$

The critical exponent β can be calculated from Monte Carlo simulations. However, the universality of critical behavior, that is, its independence of the percolating substrate, allows us to borrow its value from lattice percolation, where $\beta = 5/36$.

Cluster configuration can be characterized by the occupation numbers $\langle\nu_n\rangle$, the average numbers of clusters made of n strings. Their behavior at all values of η and n is not known. From scaling considerations in the vicinity of the phase transition, it has been found [24] that

$$\langle\nu_n\rangle = n^{-\tau}F(n^\sigma(\eta-\eta_{\rm c})), \quad |\eta-\eta_{\rm c}| << 1,\ n >> 1, \tag{17}$$

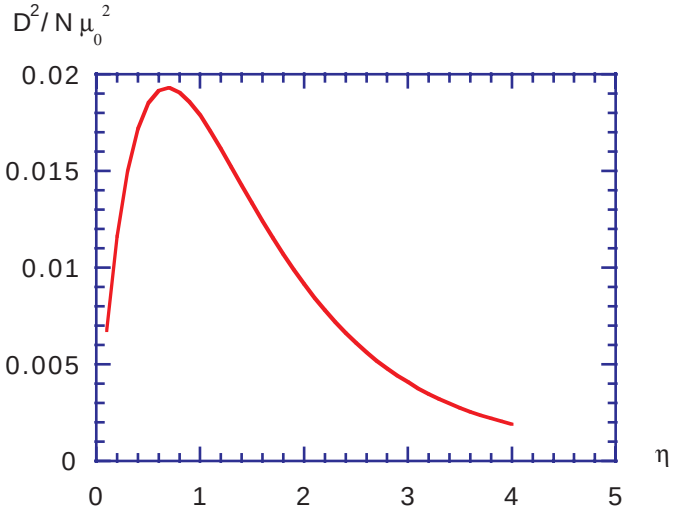

Fig. 3. Percolation dispersion squared of the multiplicity per string in units μ_0^2 as a function of η

where $\tau = 187/91$ and $\sigma = 36/91$ and the function $F(z)$ is finite at $z = 0$ and falls off exponentially for $|z| \to \infty$. Equation (17) is of limited value, since near $\eta = \eta_{\rm c}$ the bulk of the contribution is still supplied by low values of n, for which (14) is not valid. However, from (17), one can find nonanalytic parts of other quantities of interest at the transition point. In particular, one finds a singular part of the total number of clusters $M = \sum \nu_n$ as $\Delta\langle M\rangle = c|\eta - \eta_{\rm c}|^{8/3}$. This singularity is quite weak: Not only $\langle M\rangle$ itself but also its two first derivatives in η stay continuous at $\eta = \eta_{\rm c}$, and only the third blows up as $|\eta - \eta_{\rm c}|^{-1/3}$. So one should not expect that the percolation phase transition will be clearly reflected in some peculiar behavior of standard observables.

Indeed, we have observed that neither the total multiplicity nor $\langle p_{\rm T}^2 \rangle$ show any irregularity in the vicinity of the phase transition, that is, at η around unity. This is not surprising, since both quantities reflect the overlap structure rather than the cluster one. The connectedness property implied in the latter has no effect on these global observables.

It is remarkable, however, that the fluctuations of these observables carry some information about the phase transition. The dispersion of the multiplicity due to overlapping and clustering can easily be calculated in the thermodynamic limit (see the appendix). The result is shown in Fig. 3. The dispersion shows a clear maximum around $\eta = 1$ (in fact at $\eta \simeq 0.7$). So some information of the percolation phenomenon is passed to the total multiplicity, in spite of the fact that it basically does not feel the connectedness properties of the formed clusters. Of course, due to relation (10), the dispersion of $\langle p_{\rm T}^2 \rangle$ has a similar behavior.

We have to warn against a simplistic interpretation of this result. The dispersion shown in Fig. 3 is only part of the total one, which includes also contributions from the fluctuations inside the strings and also in their number. Below we shall discuss the relevance and magnitude of these extra contributions.

An intriguing question is the relation between the percolation and formation of the quark–gluon plasma. Formally, these phenomena are different. Percolation is related to the connectedness property of the strings. The (cold) quark–gluon plasma formation is related to the density of the produced particles (or, equivalently, the density of their transverse energy). However, in practice, percolation and plasma formation go together. In fact, the transverse energy density inside a single string seems to be sufficient for the plasma formation. Percolation makes the total area occupied by strings comparable to the total interaction area, thus creating a sizeable area with energy densities above the plasma formation threshold.

Let us make some crude estimates. Comparison with the observed multiplicity densities in pp($\bar{\rm p}$) collisions at present energies fix the number of produced (charged) particles per string per unit rapidity at approximately unity. Taking the average energy of each particle as 0.4 GeV (which is certainly a lower bound), the formation length in the Bjorken formula [16] as 1 fm, and the string transverse radius as 0.2 fm [7], we get the three- dimensional transverse energy density inside the string as $\sim 3{\rm GeV/fm}^3$. The plasma threshold is currently estimated to be at $1{\rm GeV/fm}^3$. So it is tempting to say that the plasma already exists inside strings. This has little physical sense, however, because of a very small area occupied by a string. One can speak of a plasma only when the total area occupied by a cluster of strings reaches a sizeable fraction of the total interaction area. In Fig. 4, we show this fraction for a maximal cluster as a function of η calculated by Monte Carlo simulations in a system of 50 strings. It grows with η and the fastest growth occurs precisely in the region of the percolation phase transition: As η grows from 0.8 to 1.2, the fraction grows from 0.3 to 0.6. With a string cluster occupying more than half of the interacting area, one can safely speak of a plasma formed in that area.

4 Dispersions and forward–backward correlations

As shown in the previous section, a definite signal for the percolation phase transition comes from the multiplicity (or $\langle p_{\rm T}^2 \rangle$) fluctuations due to string clustering. However, these fluctuations are not the only ones. An important contribution also comes from the fluctuations of the multiplicity inside the strings, or rather inside the individual overlaps of strings, which in our picture play the role of independent particle emitters. To find the total dispersion, it is convenient to use a formalism of the generating functions. Let the total probability to observe n produced particles be $\mathcal{P}(n)$. In our picture, it is given by a convolution of the probability for a given overlap configuration $P(C)$ with the probabilities for particle production from all individual overlaps:

$$\mathcal{P}(n) = \sum_C P(C) \sum_{n_1,\dots,n_M} p_1(n_1)\dots p_M(n_M)\delta_{n,\sum n_i}. \quad (18)$$

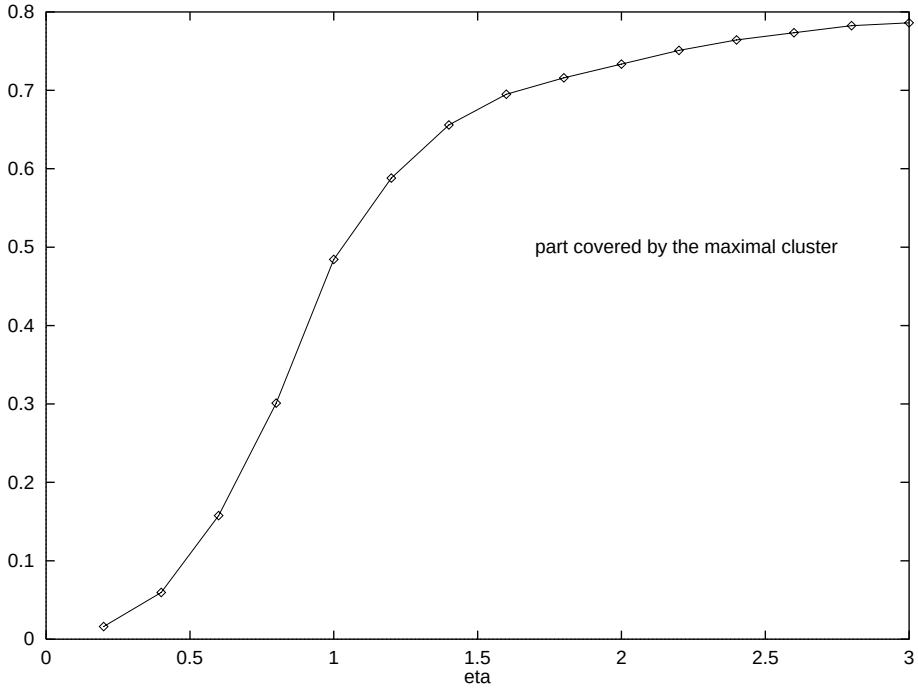

Fig. 4. Fraction of the total interaction area covered by the maximal cluster as a function of η

Here C is a "configuration", characterized by the total number of the overlaps M and their individual properties, the area and number of overlapping strings. We pass to generating functions

$$\Phi(z)=\sum_n z^n\mathcal{P}(n),\quad \phi_i(z)=\sum_n z^n p_i(n), \tag{19}$$

for which (18) transforms into

$$\Phi(z)=\sum_C P(C)\prod_i \phi_i(z). \tag{20}$$

The overall averages (with the probability $\mathcal{P}$) are given by

$$\langle n\rangle=\Phi'(z)_{z=1},\quad \langle n(n-1)\rangle=\Phi''(z)_{z=1}. \tag{21}$$

The averages inside the ith overlap are likewise given by

$$\overline{n_i}=\phi'(z)_{z=1},\quad \overline{n_i(n_i-1)}=\phi''(z)_{z=1}. \tag{22}$$

Using this formula, one readily finds the total dispersion of multiplicity as a sum of two terms,

$$D^2=D_{\rm C}^2+D_{\rm in}^2. \tag{23}$$

Here $D_{\rm C}^2$ is a dispersion due to fluctuation in configurations

$$D_{\rm C}^2=\sum_C P(C)\sum_{ik}\overline{n_i}\;\overline{n_k}-(\sum_C P(C)\sum_i\overline{n_i})^2. \tag{24}$$

It is calculated according to the distribution $\mathcal{P}$ with the assumption that the numbers of particles produced in individual overlaps are fixed to be their averages. It is this part of the dispersion which is calculated in the appendix and presented in Fig. 3. The part $D_{\rm in}^2$ is a part of the dispersion due to fluctuations inside the individual overlaps:

$$D_{\rm in}^2=\sum_C P(C)\sum_i(\overline{n_i^2}-(\overline{n_i})^2). \tag{25}$$

Its calculation is extremely difficult even in Monte Carlo simulations, since it requires identification of all individual overlaps and knowledge of their areas. To simplify, we assume that the distribution of produced particles from any overlap is Poissonian, so that $\overline{n_i^2}-(\overline{n_i})^2=\overline{n_i}$. Then we find

$$D_{\rm in}^2=\mu. \tag{26}$$

From the experimental data, we estimate $\mu_0\simeq 1.1$ for the unit rapidity interval. Comparison of Fig. 2 and Fig. 3 then shows that for the unit rapidity interval, the internal dispersion $D_{\rm in}^2$ is roughly 40 times greater than the "percolation dispersion" $D_{\rm C}^2$ at $\eta=0.7$ corresponding to the maximum for the latter. At other η, the ratio $D_{\rm in}^2/D_{\rm C}^2$ is still greater. With the growth of the rapidity interval, this ratio diminishes proportionally. However, it is obvious that one should not expect to clearly see the percolation effects directly in the observed multiplicities.

A better signal for the percolation comes from the FBC, which, as we shall see, distinguish between the percolation and intrinsic dispersions (in fact, they depend on their ratio). The FBC are described by the dependence of the average multiplicity in the backward hemisphere $\langle\mu_{\rm B}\rangle$ on the event multiplicity in the forward hemisphere $\mu_{\rm F}$. The data can be fitted by a linear expression [1]

$$\langle\mu_{\rm B}\rangle=a+b\mu_{\rm F}, \tag{27}$$

where a and b are given by expectation values

$$a=\frac{\langle\mu_{\rm B}\rangle\langle\mu_{\rm F}^2\rangle-\langle\mu_{\rm F}\mu_{\rm B}\rangle\langle\mu_{\rm F}\rangle}{\langle\mu_{\rm F}^2\rangle-\langle\mu_{\rm F}\rangle^2}, \tag{28}$$

$$b=\frac{\langle\mu_{\rm F}\mu_{\rm B}\rangle-\langle\mu_{\rm F}\rangle\langle\mu_{\rm B}\rangle}{\langle\mu_{\rm F}^2\rangle-\langle\mu_{\rm F}\rangle^2}. \tag{29}$$

In absence of the FBC, $\langle\mu_{\rm F}\mu_{\rm B}\rangle=\langle\mu_{\rm F}\rangle\langle\mu_{\rm B}\rangle$, and one obtains $a=\langle\mu_{\rm F}\rangle$ and $b=0$. Hence the strength of the correlations is given by the coefficient b.

To calculate the necessary averages, we introduce the probability $\mathcal{P}(F,B)$ to produce $F(B)$ particles in the forward (backward) hemispheres. Similarly to (18) it is given by a convolution

$$\mathcal{P}(F,B)=\sum_C P(C)\sum_{F_i,B_i}\prod_i p_i(F_i,B_i)\delta_{{\rm F},\sum F_i}\delta_{{\rm B},\sum B_i}, \tag{30}$$

which transforms into a relation between the generating functions

$$\Phi(z_{\rm F},z_{\rm B})=\sum_C P(C)\prod_i\phi(z_{\rm F},z_{\rm B}). \tag{31}$$

Instead of (21), we now have

$$\langle F\rangle=\left(\frac{\partial\Phi}{\partial z_{\rm F}}\right)_{z_{\rm F}=z_{\rm B}=1},\ \langle F(F-1)\rangle=\left(\frac{\partial^2\Phi}{\partial z_{\rm F}^2}\right)_{z_{\rm F}=z_{\rm B}=1},$$
$$\langle FB\rangle=\left(\frac{\partial^2\Phi}{\partial z_{\rm F}\partial z_{\rm B}}\right)_{z_{\rm F}=z_{\rm B}=1}, \tag{32}$$

formulas similar to the first two for B, and similar formulas for the averages over the distributions p_i inside the overlap i with the generating function $\phi_i(z_{\rm F},z_{\rm B})$. Using these formulas, we find that the dispersions again split into the percolation (C) and internal (in) parts.

$$D_{\rm F}^2=D_{\rm F,C}^2+D_{\rm F,in}^2,$$
$$D_{\rm FB}^2\equiv\langle FB\rangle-\langle F\rangle\langle B\rangle=D_{\rm FB,C}^2+D_{\rm FB,in}^2. \tag{33}$$

They are given by

$$D_{\rm F,C}^2=\sum_C P(C)\sum_{i,k}\overline{F_i}\ \overline{F_k}-(\sum_C P(C)\sum_i\overline{F_i})^2, \tag{34}$$

$$D_{\rm FB,C}^2=\sum_C P(C)\sum_{i,k}\overline{F_i}\ \overline{B_k}-\sum_C P(C)\sum_i\overline{F_i}\sum_C P(C)\sum_i\overline{B_i}, \tag{35}$$

$$D_{\rm F,in}^2=\sum_C P(C)\sum_i(\overline{F_i^2}-(\overline{F_i})^2), \tag{36}$$

$$D_{\rm FB,in}^2=\sum_C P(C)\sum_i(\overline{F_iB_i}-\overline{F_i}\ \overline{B_i}). \tag{37}$$

The usual assumption is that there are no forward–backward correlations for particle production from a single emitter (overlap i in our case). Then $D_{\rm FB,in}^2=0$. Also, from $n=F+B$, one can relate these dispersions with the overall ones $D_{\rm C}^2$ and $D_{\rm in}^2$:

$$D_{\rm F,C}^2=D_{\rm FB,C}^2=(1/4)D_{\rm C}^2,\quad D_{\rm F,in}^2=(1/2)D_{\rm in}^2. \tag{38}$$

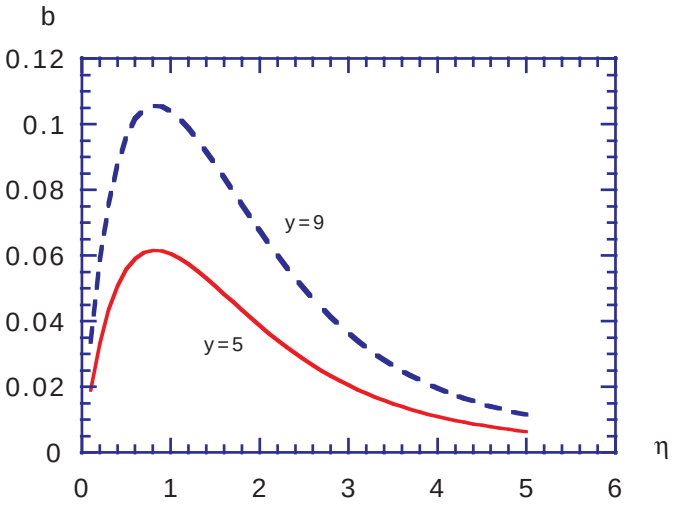

Fig. 5. Parameter b of the FBC for different rapidity intervals as a function of η for fixed N

From (29), one then finds

$$\frac{1}{b}=1+2\frac{D_{\rm in}^2}{D_{\rm C}^2}. \tag{39}$$

So, the FBC parameter b indeed measures the ratio of internal to percolation dispersions squared. If we assume that the distribution of particles produced from an individual overlap is Poissonian, then (39) transforms into

$$\frac{1}{b}=1+2\frac{\mu}{D_{\rm C}^2}. \tag{40}$$

Both μ and $D_{\rm C}^2$ grow linearly with the number of strings N, so in the thermodynamic limit, b does not depend on N. However, it depends on the multiplicity of a single string μ_0, since μ is proportional to μ_0 and $D_{\rm C}^2$ is proportional to μ_0^2. As has been mentioned, we find from the experimental data that $\mu_0\simeq 1.1\,y$, where y is the rapidity interval of the produced particles. So the right-hand side of (40) falls with the growth of the rapidity window. It also has a minimum at $\eta\sim 0.7$ corresponding to the maximum $D_{\rm C}^2$. From this we see that the FBC parameter b also has a maximum near $\eta\sim 0.7$, whose magnitude grows with the rapidity interval. In Fig. 5, we show the behavior of b as a function of η for two rapidity intervals $y=5$ and $y=9$.

One can also study the FBC for $\langle p_{\rm T}^2\rangle$. Owing to relation (8), for fixed N they are uniquely determined by the fluctuations in μ. It is convenient to choose the inverse $\langle p_{\rm T}^2\rangle$ as an observable:

$$\tau=\frac{\mu_0\langle p_{\rm T}^2\rangle_0}{\langle p_{\rm T}^2\rangle}=\frac{\mu}{N}. \tag{41}$$

Then it is obvious that the parameter b for τ is the same as for the multiplicity, since both percolation and internal dispersions for τ are obtained from those for μ, divided by N. However this equivalence holds only for a fixed number

of strings N. In the realistic situation, N fluctuates. The multiplicity is an extensive observable and carries these fluctuations directly. The result is that they are large and smear out nearly all traces of percolation. In contrast, τ is an intensive observable and so feels the fluctuation in N only indirectly, through the fluctuations in the parameter η. As a result, the percolation effects for the FBC in τ are clearly visible, as we shall see in the next section.

5 Realistic hadronic and nuclear collisions

For realistic hadronic and nuclear collisions, the total number of strings N grows with energy and fluctuates. For pp collisions, the initial number of color strings N created at a given c.m. energy $\sqrt{s}$ can be taken from the well-known calculations of [1,2]. For pA and AB collisions, this number should be multiplied by the effective number of collisions C. At asymptotic energies for minimum-bias hA and AB collisions, the AGK rules predict

$$C_{\rm A} = A\sigma/\sigma_{\rm A}, \quad C_{\rm AB} = AB\sigma/\sigma_{\rm AB}, \tag{42}$$

where σ ($\sigma_{\rm A}$, $\sigma_{\rm AB}$) is the inelastic pp (pA, AB) cross section. For hA collisions at fixed impact parameter b,

$$C_{\rm A} = A\sigma T_{\rm A}(b)/(1-\exp(-A\sigma T_{\rm AB})), \tag{43}$$

where $T_{\rm A}$ is the standard nuclear profile function (normalized to unity). The same relation holds for AB collisions in the optical approximation with

$$A\to AB, \quad T_{\rm A}\to T_{\rm AB}(b) = \int {\rm d}^2c\, T_A(c)T_B(b-c). \tag{44}$$

The transverse interaction area for pp and hA collisions obviously is of the order σ. For AB collisions, it depends on the geometry of the collisions. We restrict ourselves to central ($b=0$) collisions of identical nuclei, when evidently the interaction area is $\sigma_{\rm AA}$. The parameter η is then calculated according to (11). We have taken the string area σ_0 as

$$\sigma_0 = \pi a^2, \quad a = 0.2 \text{ fm}. \tag{45}$$

in accordance with arguments presented in [7]. To relate the multiplicity to the experimental data, we normalized μ to the observable central (charged) multiplicity per unit rapidity in pp collisions at low energies. This fixes μ_0 for the unit rapidity to be 1.1. The found values of $\mu \equiv ({\rm d}n^{\rm ch}/{\rm d}y)_{y=0}$ are presented in the table for central S–S and Pb–Pb collisions (fourth column) together with the corresponding values of c.m. energy $\sqrt{s}$, η, and number of strings N (first, second, and third columns, respectively). To compare, we present the values of μ found without fusion and percolation (independent-string picture) in the seventh column. One should have in mind that the asymptotic formulas for the number of collisions (42)–(44) used to determine the number of strings are not valid at comparatively low energies because of restrictions imposed by energy conservation. As stated in [1], at lower energies, the number of collisions can be roughly obtained by the multiplication of (42)– (44) by a factor of 1/2. Correspondingly, our values for the multiplicity at two lower energies have to be corrected for energy conservation by a factor of this order. We preferred not to make this correction, since, in any case, it cannot be determined with any degree of rigor, and the effects we are considering are essential only at high enough energies, where (42)–(44) are, as we hope, valid.

Table 1. Columns show, from left to right: c.m. energy per nucleon $\sqrt{s}$; parameter η (1); number of initially produced strings N; central charged multiplicity per unit rapidity μ and its FBC parameter $B(\mu)$; the FBC parameter for the inverse $\langle p_{\rm T}^2\rangle$, $b(\tau)$; and the multiplicities and $b(\mu)$ in the independent-string model (subscript 0)

S–S scattering ($b=0$)

$\sqrt{s}$	η	N	μ	$b(\mu)$	$b(\tau)$	μ_0	b_0
19.4	0.33	99	101	0.67	0.04	111	0.65
62.5	0.47	143	140	0.74	0.08	160	0.72
200	0.65	198	185	0.79	0.13	221	0.77
546	0.84	255	228	0.82	0.18	284	0.80
1800	1.10	336	283	0.85	0.24	374	0.82
7000	1.47	448	349	0.87	0.30	499	0.85

Pb–Pb scattering ($b=0$)

$\sqrt{s}$	η	N	μ	$b(\mu)$	$b(\tau)$	μ_0	b_0
19.4	1.45	1530	1200	0.69	0.13	1700	0.65
62.5	2.09	2200	1530	0.75	0.19	2450	0.72
200.0	2.88	3040	1870	0.78	0.25	3390	0.77
546.0	3.72	3920	2170	0.80	0.28	4370	0.80
1800.0	4.90	5170	2530	0.81	0.31	5760	0.82
7000.0	6.53	6890	2940	0.82	0.33	7680	0.85

As we observe, percolation considerably damps the multiplicity at high energies, from nearly 8000 at $\sqrt{s}=$ 7000 GeV for central Pb–Pb collision down to approximately 3000. This effect was predicted in our earlier papers on string fusion [11,12] and is now reproduced in various models [17].

As to the FBC, we studied them both for the multiplicity and the inverse $\langle p_{\rm T}^2\rangle$ (in fact for the observable τ, defined in (41)). We have taken one half of the total rapidity available for the relevant rapidity window. The "external" dispersion in the denominator of (39) has to include also the fluctuations in the number of strings. We have assumed the overall distribution in N to be Poissonian, so that $\Delta N/N = 1/\sqrt{N}$. As has been mentioned, for the multiplicity, because of its extensive character, the dispersion in N simply adds to $D_{\rm C}$. It is large and absolutely dominates all other contributions. So it is no surprise that the coefficient b for the multiplicity with percolation (fifth column in the table) differs only slightly from the one without percolation (eighth column).

In contrast, for τ, the fluctuations in N only enter via the dependence of η on N. The result is that they

are smaller than the percolation contribution at the maximum of the latter but fall with η more slowly, so that they dominate at large η. As a result, the characteristic peaked form of the parameter b found at fixed N (Fig. 5) disappears and b results steadily growing with η (sixth column in the table). However, one should note that in the independent-string picture, the parameter b for τ is zero, since the dependence on N is then completely absent. So experimental study of the FBC for inverse $\langle p_{\rm T}^2\rangle$ seems to be a promising way to observe signatures of string fusion and percolation.

6 Conclusions

In this study, we have analyzed the impact of fusion and percolation of color strings on global observables, such as multiplicities and $\langle p_{\rm T}^2\rangle$. To do this, a certain dynamical assumption has been made. The strings have been assumed to decay into the observed hadrons independently in each overlap.

On the qualitative level, the results are best seen in the idealized case of a fixed number of strings $N >> 1$ (equivalent to plasma studies in the thermodynamic limit). A clear consequence of fusion and percolation is damping of the multiplicities, which is well described by a damping factor (15) that follows from the percolation theory. An unexpected but potentially important result is that the parameter b of the FBC shows a clear maximum at the percolation point. Such a maximum would be natural in fluctuations, of, e.g., the cluster sizes, where it is to be expected as a signature of the percolation phase transition. However, multiplicities do not seem to feel directly the cluster structure, so that the appearance of the maximum in their fluctuations is a new result.

In the realistic case of nuclear collisions, where N fluctuates, the predicted multiplicities repeat the pattern observed at fixed N and are damped by the same factor (15). At LHC energies, it reduces the multiplicities by more than two times. However, the parameter b for multiplicity is completely dominated by fluctuations in the number of strings and so is only slightly different from the one in the independent-string picture. A better (intensive) observable for seeing the impact of percolation is $\langle p_{\rm T}^2\rangle$ or its inverse, for which the contribution of the fluctuations in N is drastically reduced. For $\langle p_{\rm T}^2\rangle^{-1}$ we predict sizeable values of b to be contrasted with $b = 0$ in the independent-string picture. Observation of nonzero values of b for $\langle p_{\rm T}^2\rangle^{-1}$ would therefore be a clear signature of string fusion and percolation.

Acknowledgements. M.B. thanks the University of Santiago de Compostela for hospitality. C.P. thanks the Institute for Nuclear Theory of the University of Washington for hospitality. This study was supported by the NATO grant CRG.971461.

Appendix
Multiplicities and their dispersion

Let us recall the geometry of our percolation picture. Discs of radius a and area $\sigma_0 = \pi a^2$ are homogeneously distributed in the total area S. It is assumed that centers of the discs are inside the unit circle of area $S_0 = \pi$ so that $S = \pi(1+a)^2$. The disc density is $\rho = N/S$, and the percolation parameter is $\eta = \rho\sigma_0 = N\sigma_0/S$. In the thermodynamic limit, $N \to \infty$, so that at fixed η, the radius of the discs goes to zero. For fixed η,

$$a = \left(\sqrt{\frac{N}{\eta}} - 1\right)^{-1}, \tag{46}$$

so that at large N, $a \sim 1/\sqrt{N}$ and $\sigma_0 \sim 1/N$. Since the discs are distributed homogeneously, the probability that their centers are at points r_i $(i = 1, ..., N)$ inside the unit circle is independent of r_i and is given by

$$P(r_i) = S_0^{-N}. \tag{47}$$

Let us take a configuration which corresponds to the disc centers at points r_i. Then the overlap area of exactly n discs is given by the integral

$$\begin{aligned} &S_n(r_1, ..., r_N) \\ &\quad = \int_S {\rm d}^2 r \sum_{\{i_1,...,i_n\}\subset\{i_1,...,i_N\}} \prod_{k=1}^{n} \theta(a - |\mathbf{r} - \mathbf{r}_{i_k}|) \\ &\qquad \times \prod_{k=n+1}^{N} \theta(|\mathbf{r} - \mathbf{r}_{i_k}| - a). \end{aligned} \tag{48}$$

The average of S_N will be given by a multiple integral over r_i with the probability (47):

$$\begin{aligned} \langle S_n\rangle &= \frac{1}{S_0^N} \int_{S_0} \prod_{i=1}^{N} {\rm d}^2 r_i S_n(r_1, ..., r_N) \\ &= C_N^n \int_S {\rm d}^2 r F^n(r)(1 - F(r))^{N-n}, \end{aligned} \tag{49}$$

where

$$F(r) = (1/S_0) \int_{S_0} {\rm d}^2 r_1 \theta(a - |\mathbf{r} - \mathbf{r}_1|). \tag{50}$$

The function $S_0 F(r)$ gives an area occupied by a circle C of radius a with a center at r which is inside the unit circle S_0. If $r < 1 - a$, then C is always inside S_0, so that

$$F(r) = \sigma_0/S_0, \quad 0 < r < 1 - a. \tag{51}$$

However, for $r > 1 - a$ a part of C turns out to be outside the unit circle, and

$$F(r) = \sigma(r)/S_0, \quad 1 - a < r < 1 + a, \tag{52}$$

where $\sigma(r) \le \sigma_0$ is the overlap of the two discs C and S_0.

Generally, an overlap of two circles of radii r_1 and r_2 with a distance r between their centers is given by

$$\sigma(r_1,r_2,r) = (1/2)r_1^2(\alpha_1-\sin\alpha_1) + (1/2)r_2^2(\alpha_2-\sin\alpha_2), \quad (53)$$

where

$$\cos(\alpha_1/2) = \frac{1}{2r_1}\left(r+\frac{r_1^2-r_2^2}{r}\right),$$
$$\cos(\alpha_2/2) = \frac{1}{2r_2}\left(r-\frac{r_1^2-r_2^2}{r}\right). \quad (54)$$

The function $\sigma(r)$ in (52) is just $\sigma(1,a,r)$.

Formulas (49)–(54) allow one to calculate numerically the average $\langle S_n\rangle$ for any finite value of N without much difficulty.

In the thermodynamic limit $N\to\infty$ where η is fixed, the calculation of $\langle S_n\rangle$ becomes trivial. Indeed, then one can neglect the part of integration in r with $r>1-a$ altogether, with an error $\sim 1/a\sim 1/\sqrt{N}$. With the same precision, one then finds

$$\langle S_n\rangle = SC_N^n(\sigma_0/S)^n(1-\sigma_0/S)^{N-n}, \quad (55)$$

where we have set $S_0\simeq S$. The physically relevant values of n remain finite as $N\to\infty$. So we can approximately take

$$C_N^n = N^n/n!, \quad (1-\sigma_0/S)^{N-n} = \exp(-N\sigma_0/S). \quad (56)$$

We then find that in the thermodynamic limit the distribution of overlaps in n is Poissonian with the mean value given by η (13).

Calculation of the multiplicity dispersion requires knowledge of the average of its square. With the centers of the discs at $r_1,...,r_N$, it has the form

$$\mu^2(r_1,...,r_N) = (1/\sigma_0^2)(\sum_n \sqrt{n}S_n(r_1,...,r_N))^2, \quad (57)$$

where $S_N(r_1,...,r_N)$ is given by (48). Taking the average over the discs' center positions, we now come to a double integral in r and r':

$$\langle\mu^2\rangle = \frac{1}{\sigma_0^2}\sum_{m,n}\sqrt{mn}\int_S {\rm d}^2r{\rm d}^2r'\frac{1}{S_0^N}\int_{S_0}\prod_{i=1}^N {\rm d}^2r_i$$
$$\sum_{\{i_1,..i_n\}\subset\{1,...,N\}}\prod_{k=1}^n\theta(a-|\mathbf{r}-\mathbf{r}_{i_k}|)\prod_{k=n+1}^N\theta(|\mathbf{r}-\mathbf{r}_{i_k}|-a)$$
$$\sum_{\{j_1,...,j_m\}\subset\{1,...,i\}}\prod_{l=1}^m\theta(a-|\mathbf{r}-\mathbf{r}_{j_l}|)\prod_{l=m+1}^N\theta(|\mathbf{r}-\mathbf{r}_{j_l}|-a). \quad (58)$$

This complicated expression, however, continues to be factorized in all r_i. Let us assume for the moment that $n\ge m$. We can always rename the variables r_i to have in the first sum $r_1,...,r_n$ as variables in the first product of θ functions (and as a result, the rest of the $N-n$ variables $r_{n+1},...,r_N$ go into the second product). We shall then have C_N^n terms with the identical first sum. Now let p variables in the first product of θ functions in it coincide with p variables from the set $r_1,...,r_n$. We have C_n^p of such terms, which will evidently all have the same dependence on the mentioned p variables. The left $m-p$ variables from the first product of θ functions in the second sum do not coincide with any variables $r_1,...,r_n$, so they are chosen fro variables $r_{n+1},...,r_N$. We shall have C_{N-n}^{m-p} various terms of this sort. Thus the overall symmetry factor turns out to be a multibinomial coefficient,

$$C_N^nC_N^pC_{n-n}^{m-p} = \frac{N!}{p!(n-p)!(m-p)!(n-n-m+p)!} \equiv C_N^{p,n-p,m-p}. \quad (59)$$

This coefficient multiplies the result of integration over all r_i, $i=1,...,N$, which has the form (at fixed r and r')

$$\phi^p(r,r')\chi^{n-p}(r,r')\chi^{m-p}(r',r)\zeta^{N-n-m+p}(r,r'), \quad (60)$$

where

$$\phi(r,r') = (1/S_0)\int_{S_0}\theta(a-|\mathbf{r}-\mathbf{r}_1|)\theta(a-|\mathbf{r}'-\mathbf{r}_1|),$$
$$\chi(r,r') = (1/S_0)\int_{S_0}\theta(a-|\mathbf{r}-\mathbf{r}_1|)\theta(|\mathbf{r}'-\mathbf{r}_1|-a) = F(r)-\phi(r,r'),$$
$$\zeta(r,r') = (1/S_0)\int_{S_0}\theta(|\mathbf{r}-\mathbf{r}_1|-a)\theta(|\mathbf{r}'-\mathbf{r}_1|-a) = 1-F(r)-F(r')+\phi(r,r'), \quad (61)$$

with $F(r)$ defined before by (50). Of course one should sum over all possible values of p.

Combining all the terms, we find the expression for the average square of multiplicity as

$$\langle\mu^2\rangle = \frac{1}{\sigma_0^2}\sum_{n,m,p}\sqrt{(n+p)(n+p)},$$
$$C_N^{n,m,p}\int_S d^2rd^2r'\phi^p(r,r')\chi^n(r,r') \times\chi^m(r',r)\zeta^{N-n-m-p}(r,r'). \quad (62)$$

This expression is exact and may serve as a basis for the calculation of the average square of the multiplicity at finite N. However, the new function ϕ becomes very complicated when both variables r and r' are greater than $1-a$ (it is then given by the overlap area of three circles, and we do not know any simple analytic expression for it).

For this reason rather than analyze the general expression (62) for finite N, we shall immediately take the thermodynamic limit $N\to\infty$. We are in fact interested in the dispersion, not in the average square of multiplicity; it is important, since the leading terms in N cancel in the dispersion. So we shall study the difference

$$D^2 = \langle\mu^2\rangle - \langle\mu\rangle^2 \quad (63)$$

in the limit $N\to\infty$, η finite. As we shall see, although both terms in the right-hand side of (63) behave as N^2 separately, their difference grows only as N.

Separating from (62) the term with $p=0$ and combining it with the second term on the right-hand side of (63), we present the total dispersion squared as a sum of two terms,

$$D^2 = D_1^2 + D_2^2, \tag{64}$$

where

$$\begin{aligned} D_1^2 = \frac{1}{\sigma_0^2}\sum_{n,m}\sqrt{nm}\int_S \mathrm{d}^2r\mathrm{d}^2r'[C_N^{n,m}\chi^n(r,r') \\ \times\chi^m(r',r)\zeta^{N-n-m}(r,r') - C_N^nC_N^mF^n(r)F^M(r') \\ \times(1-F(r))^{N-n}(1-F(r'))^{N-m}], \end{aligned} \tag{65}$$

and D_2^2 is given by (62) with a restriction $p\geq 1$.

Function $S_0\phi(r,r')$ gives the overlapping area of three circles: The unit circle S_0 and two circles C and C' of radii a with centers at r and r'. It is evidently zero if $R=|\mathbf{r}-\mathbf{r}'|>2a$, since for such R, circles C and C' do not overlap. Because of this, in the part D_2^2, which has at least one factor ϕ, the integration in r and r' is restricted to the domain $R<2a$, whereas in the part D_1^2, the integration covers the whole range of values of R.

We begin with the part D_1^2. Splitting the integration region in r and r' in two parts, $R>2a$ and $R<2a$, we make use of (61) and present the first part as

$$\begin{aligned} D_{11}^2 = \frac{1}{\sigma_0^2}\sum_{n,m}\sqrt{nm}\int_{R>2a}\mathrm{d}^2r\mathrm{d}^2r'F^n(r)F^m(r') \\ \times[C_N^{n,m}(1-F(r)-F(r'))^{N-n-m} - C_N^nC_N^m \\ \times(1-F(r))^{N-n}(1-F(r'))^{N-m}]. \end{aligned} \tag{66}$$

One notices immediately that the in the thermodynamic limit the leading terms in the integrand (independent of N) cancel, and only terms of the order $1/N$ remain. The integration over r and r' provides a factor $\propto N^2$ so that the total contribution results $\propto N$. To find this term, we use that at large N, up to terms of the order $1/N^2$,

$$C_N^n = \frac{N^n}{n!}\left(1-\frac{n(n-1)}{2N}\right),$$

$$C_N^{m,n} = \frac{N^{n+m}}{n!m!}\left(1-\frac{(m+n)(m+n-1)}{2N}\right),$$

$$(1-F)^{N-n} = e^{-NF}(1+nF-NF^2/2),$$

where we have taken into account that F has order $1/N$. Then we obtain

$$\begin{aligned} D_{11}^2 = \frac{1}{\sigma_0^2}\sum_{n,m}\frac{\sqrt{nm}}{n!m!}N^{n+m} \\ \times\int_{R>2a}\mathrm{d}^2r\mathrm{d}^2r'F^n(r)F^m(r') \\ \times\exp(-N(F(r)+F(r')) \\ \times(mF(r)+nF(r')-NF(r)F(r')-nm/N). \end{aligned} \tag{67}$$

The integrand is now explicitly of the order $1/N$, so that we can change the integration region to $r,r'<1-a$, since the difference in the area will be of the order $a^2\sim 1/N$, which results in the overall difference of the order $1/N^2$ and can safely be neglected. In the region $r,r'<1-a$, both $F(r)$ and $F(r)$ are constants, given by (51). Integration over r and r' gives an overall factor S^2, so that in the end, we get

$$\begin{aligned} D_{11}^2/N &= \frac{1}{\eta^2}\mathrm{e}^{-2\eta}\sum_{n,m}\frac{\eta^{n+m}}{n!m!}\sqrt{nm}[\eta(n+m)-\eta^2-nm] \\ &= -\frac{(\eta\langle\sqrt{n}\rangle - \langle n\sqrt{n}\rangle)^2}{\eta^2}. \end{aligned} \tag{68}$$

In the last expression, the averages are to be taken over the Poissonian distribution with the mean value η. The part D_{11}^2 is thus negative (and results are comparatively small for all values of η).

In the second part of D_1^2, the integration goes over a small region $R<2a$, of the order $a^2\sim 1/N$, so that one can retain only the leading terms in the integrand. Moving to the integration over r and R, one observes that at fixed $r<1-a$, the integration region over R covers the whole region $R<2a$. For $r>1-a$ the integration region in R becomes much more complicated, determined by the condition $r'=|\mathbf{r}+\mathbf{R}|<1+a$. However, the contribution from the latter region will be of the order $a^3\sim 1/N\sqrt{N}$, since apart from a factor $\propto a^2$ from the integration over R, a factor $\propto a$ appears due to integration over $r>1-a$. Thus, up to terms of the relative order $1/\sqrt{N}$, we can neglect the contribution from the region $r>1-a$.

If $r<1-a$, the circle C is completely inside the unit circle S_0. Then its intersection with the circle C' is also automatically inside S_0. Therefore function $S_0\phi(r,r)$ in this region is simply given by the overlap of the circles C and C', that is $\sigma(a,a,R)$ defined by (53). We thus find

$$\phi(r,r') = \frac{\sigma_0}{S}\lambda(R), \tag{69}$$

where

$$\lambda(R) = (1/\pi)(\alpha-\sin\alpha),\quad \alpha = 2\arccos(R/2). \tag{70}$$

Putting this into the expression for D_{12}^2 and retaining the leading terms in the limit $N\to\infty$, we obtain

$$\begin{aligned} D_{12}^2/N = \frac{2}{\eta}\mathrm{e}^{-2\eta}\sum_{n,m}\frac{\sqrt{nm}}{n!m!}\eta^{n+m} \\ \times\int_0^2 R\mathrm{d}R[(1-\lambda(R))^{n+m}\mathrm{e}^{\eta\lambda(R)}-1]. \end{aligned} \tag{71}$$

This expression can be easily evaluated numerically. It is relatively large and also negative.

We finally come to the part D_2^2. The integration in r,r' goes over $R<2a$, so that we can apply the same approximations as made in calculating D_{12}^2. We find

$$D_2^2/N = \frac{2}{\eta}\mathrm{e}^{-2\eta}\sum_{n,m}\sum_{p=1}\frac{\sqrt{(n+p)(m+p)}}{n!m!p!}\eta^{n+m+p}$$

$$\times \int_0^2 R{\rm d}R\lambda^p(R)(1-\lambda(R))^{n+m}{\rm e}^{\eta\lambda(R)}. \quad (72)$$

This part is evidently positive. Its numerical evaluation shows that it nearly cancels the large negative contributions from D_1^2 (in fact, four digits are canceled typically). Thus the numerical calculation of the dispersion requires some care.

References

1. A. Capella, U.P. Sukhatme, C.-I. Tan, J. Tran Thanh Van, Phys. Lett. B **81**, 68 (1979); Phys. Rep. **236**, 225 (1994)
2. A.B. Kaidalov, K.A. Ter-Martirosyan, Phys. Lett. B **117**, 247 (1982)
3. B. Andersson, G. Gustafson, B. Nilsson-Almqvist, Nucl. Phys. B **281**, 289 (1987)
4. K. Werner, Phys. Rep. **232**, 87 (1993)
5. M. Gyulassy, CERN preprint CERN-TH 4794 (1987)
6. H. Sorge, H. Stoecker, W. Greiner, Nucl. Phys. A **498**, 567c (1989)
7. N. Armesto, M.A. Braun, E.G. Ferreiro, C. Pajares, Phys. Rev.Lett. **77**, 3736 (1996)
8. M.A. Braun, C. Pajares, J. Ranft, Santiago de Compostela preprint US-FT/24-97, hep-ph/9707363
9. M. Nardi, H. Satz, Bielefeld preprint BI-TP 98/10, hep-ph/9805297; H. Satz, Bielefeld preprint BI-TP 98/11, hep-ph/9805418
10. T.S. Biro, H.B. Nielsen, J. Knoll, Nucl. Phys. B **245**, 449 (1984)
11. M.A. Braun, C. Pajares, Phys. Lett. B **287**, 154 (1992); Nucl. Phys. B **390** 542, 549 (1993)
12. N.S. Amelin, M.A. Braun, C. Pajares, Phys. Lett. B **306** 312 (1993); Z. Phys. C **63**, 507 (1994)
13. A. Bialas, W. Czyz, Nucl. Phys. B **267**, 242 (1986)
14. D. Stauffer, Phys. Rep. **54**, 2 (1979)
15. M.B. Isichenko, Rev. Mod. Phys.**64**, 961 (1992)
16. J.D. Bjorken, Phys. Rev D **27**, 140 (1983)
17. See, e.g., A. Capella, A. Kaidalov, J. Tran Thanh Van, Orsay preprint LPT ORSAY 99-15, hep-ph/9903244